Author Manuscript

Author Manuscript

Author Manuscript

Author Manuscript

HHS Public Access

Author manuscript

Fuel (Lond). Author manuscript; available in PMC 2020 June 10.

Published in final edited form as:

Fuel (Lond). 2019 December 15; 258: . doi:10.1016/j.fuel.2019.116020.

Physicochemical and mineralogical characterization of biomass ash from different power plants in the Upper Rhine Region

Christoph Maschowski[a,*], **Peter Kruspan**[b], **Patxi Garra**[c], **Ali Talib Arif**[d,e], **Gwenaëlle Trouvé**[c], **Reto Gieré**[f]

[a]Institute of Earth and Environmental Sciences-Geochemistry, University of Freiburg, D-79104 Freiburg, Germany [b]LafargeHolcim Ltd, Zürcherstrasse 156, 8645 Jona, Switzerland [c]Laboratoire Gestion des Risques et Environnement (LGRE), Université de Haute-Alsace, F-68093 Mulhouse Cedex, France [d]Institute for Infection Prevention and Hospital Epidemiology, University Medical Center Freiburg, University of Freiburg, Faculty of Medicine, University of Freiburg, D-79106 Freiburg, Germany [e]Kurdistan Institution for Strategic Studies and Scientific Research (KISSR), Qirga, Sulaimani, Iraq [f]Department of Earth and Environmental Science and Center of Excellence in Environmental Toxicology, University of Pennsylvania, Philadelphia, PA 19104-6316, USA

Abstract

Bottom and fly ash samples from six biomass power plants with different power scales and various flue gas treatment strategies were collected and analyzed in regard to their mineralogical composition, and their bulk major and trace element contents, all of which are of concern for regulations on biomass ash for further utilization. Furthermore, individual ash particles were investigated by scanning electron microscopy to characterize their physicochemical microstructures.

Thermal behavior of wood-pellet ash, i.e. decomposition processes and mineral transformations during combustion, was indicated by thermogravimetric analysis and X-ray diffraction.

Results reveal extensive variation of physicochemical features across the different ash types: wood-chip fly ash from electrostatic precipitators mainly consisted of water-soluble salts, whereas wood-chip fly ash from cyclones contained predominantly cenospheres (hollow spherical fly ash particles) and higher heavy metal concentrations. In addition, the fuel type and admixture had influences on ash compositions; some fuels like Miscanthus straw require a liming agent such as calcium hydroxide to be admixed to prevent fouling, which is then predominantly found in the ash. Furthermore, boiler size had an influence on fly ash composition. Cadmium concentrations were elevated in some fly ash samples at levels of concern for further utilization, whereas concentrations of troublesome Cr(VI) were below the detection limit for all investigated ash samples. Other contaminating elements such as Ni, Pb and Zn were variable but below limit values.

*Corresponding author. christoph@maschowski.de (C. Maschowski).

Appendix A. Supplementary data

Supplementary data to this article can be found online at https://doi.org/10.1016/j.fuel.2019.116020.

Author Manuscript Author Manuscript Author Manuscript Author Manuscript

Results clearly show that the nature of biomass ash calls for careful analyses prior to further application as, e.g., cement clinker replacement material.

Keywords

Biomass; Ash; Wood ash; Recycling

1. Introduction

For the last decades, the energetic use of wood has become an important factor for the switchover from fossil to renewable fuels across all scales of combustion devices and power plants. The accumulating ashes could be used as alternative clinker replacement materials (CRM) in cement production, thus potentially reducing the industry's substantial greenhouse gas emissions [33]. Especially fly ash (FA) of wood from medium- and large-scale power plants is produced in large amounts and often has similar (pozzolanic) properties as ash from coal combustion, which is a widely used CRM [12]. Nevertheless, the composition and the quality of coal FA are fairly constant, because coal-fired power plants are large-scale combustors burning standardized fuel at constant combustion parameters, and the FA is trapped by standardized flue gas treatment devices. In contrast, FA from biomass power plants exhibits large variations in composition and morphology, depending on fuel type, scale of the power plant, and flue gas treatment strategy [26,37]. Fuel from biomass is of disparate nature; depending on local availability of the biomass, fuel types ranging from straw and forest residues to wood chips and standardized wood pellets exist. Standardized wood pellets are the most homogenous wood fuel type and are predominantly used for direct combustion in small-scale combustors, or gasified for electrical power generators. Nevertheless, the most common type of biomass fuel for medium-scale combustors is wood chips, which consist of chopped wood, several centimeters in size, and which can be made from various tree species. Large-scale biomass power plants are designed for combustion of a wide range of biomass fuel types or for co-combustion with non-biomass fuels [23]. To achieve optimized combustion conditions, large-scale biomass combustion facilities in many cases use fluidized bed technology. Such fluidized beds improve burning conditions for heavy loads of solid fuel and promote complete combustion. The additives, commonly consisting of limestone, contribute to the final composition of the FA (dust) trapped downstream from the flue gas [10] and the corresponding FAs are extremely rich in Ca [14]. In large-scale biomass power plants, a mixture of wood and organic waste materials such as crop residues is often used as fuel.

To avoid corrosion of the boiler, or slagging and fouling of the heat exchanger and flue gas pipes and tube walls, calcium hydroxide (Ca (OH)2) is typically added, especially when high-K biomass is used, such as straw from graminaceous fuels like Miscanthus [20]. It is therefore very unlikely to obtain ash from pure Miscanthus combustion at a power plant due to the need of calcium hydroxide amendment. The strategy of flue gas treatment also depends on the type and size of the biomass power plant. Dust emission limits for biomass combustion are regulated by law, e.g. in Germany [5] or Switzerland [28], and according to these regulations, the use of flue gas treatment devices is necessary. Small-scale combustors

Author Manuscript Author Manuscript Author Manuscript Author Manuscript

(< 500 kW) are typically equipped only with cyclones/multi-cyclones (CYC), i.e. passive dust traps with no need for electrical power. Medium-scale combustors (500 kW-5 MW) typically use electrostatic precipitators (ESP), because they have higher collecting efficiencies and are capable of trapping smaller particles. To increase the efficiency of an ESP, a cyclone is in many cases connected upstream. Large-scale biomass power plants (> 5 MW) generally use a combination of cyclones, electrostatic precipitators and/or additional bag-house filters [13]. Bag-house filters need lots of space and demand filter cleaning protocols. Furthermore, large-scale power plants may have additional sprayers, catalyzers and activated-carbon filters to remove gas contaminants, such as CO, SO_2, NO_X and gaseous heavy metals (e.g. Hg) or arsenic (As) from the flue gas. In summary, FAs from biomass combustion are expected to be complex materials with diverse compositions and morphologies, which means that they are by default not ready for use as valuable CRM [2].

For extensive future utilization of biomass ashes as CRM, it is therefore important to understand the interdependencies of combustion parameters and to identify the most valuable ash type. With this information at hand, the biomass combustion industry will have the means to consider their FA as input material for the cement industry by fully taking into account the appropriate requirements on fuel type and quality, additives used and flue gas treatment strategy for FA trapping.

The aim of this study was to contribute to the regional development of waste management in the Upper Rhine Region and simultaneous reduction of greenhouse gas emissions from the cement industry. The characterization through physicochemical parameters of different biomass ash samples, collected from different power plants burning locally available fuel types, can be used to evaluate their possible use as secondary raw materials and in particular for interpretations of cement tests, which were conducted on the same samples and reported in a separate study [19].

2. Materials and methods

2.1 Biomass ash samples

Fly ash (FA) and bottom ash (BA) samples from six power plants in the Upper Rhine Region (Germany and France) with various flue gas treatment strategies were collected in 2014. The power plants burn either wood chips, made from mostly locally available soft wood, or Miscanthus straw. The location, fuel and boiler type of the power plants and their corresponding flue gas treatment strategies are listed in Table 1. A simplified schematic drawing of a typical biomass combustion facility is shown in Fig. S1 (Supplementary Materials), which also displays different flue gas treatment strategies as well as the corresponding ash collection points. All ash samples were collected directly during full operation of the boilers and therefore, complete combustion under ideal conditions can be assumed. In the case of St. Peter, temperatures were 765 °C in the combustion chamber and about 910 °C in the flue gas. Fly ashes and one BA were analyzed in terms of microstructure, morphology, elemental compositions and mineralogical species. Characterization methods were chosen to assess the possible applicability of the ashes as CRM and their effects on mortar strength (see separate study by [19]).

Author Manuscript Author Manuscript Author Manuscript Author Manuscript

In addition, ash of standard wood pellets (DIN+, a combination of the German DIN 51,731 standard and the Austrian OENORM M 7135 standard) was produced in a 40 kW multi-fuel boiler (HKRST/V-FSK) supplied by REKA® (Aars, Denmark) at the Laboratoire de Gestion des Risques et Environnement (LGRE), University of Mulhouse. To help understanding thermal conversion processes of solid phases in wood ash, thermogravimetric analysis was conducted on this ash of standard wood pellets in a box-type electric laboratory furnace supplied by Thermo Fischer Scientific (Waltham, Massachusetts).

2.2. Physical, chemical and mineralogical analyses

The investigated ashes were characterized by mineralogical and chemical analytical methods. Mineral phases were identified via X-ray diffraction (XRD) including Rietveld refinement in order to determine semi-quantitative concentrations of the phases present. XRD was also conducted on reference ash samples from thermogravimetric analysis (TGA). Concentrations of the main chemical constituents of the ashes were determined by X-ray fluorescence spectroscopy (XRF). Inductively coupled plasma-mass spectrometry (ICP-MS) and inductively coupled plasma-atomic emission spectrometry (ICP-AES) were carried out on ash samples to obtain concentrations of trace elements of concern for biomass ashes used in cement according to [36,29]. Total organic carbon (TOC) was estimated by using a LECO carbon analyzer. Microstructures of the ashes were investigated by scanning electron microscopy (SEM), whereas the chemical composition of individual ash particles was studied by combining SEM with energy-dispersive X-ray spectroscopy (SEM-EDX).

2.2.1. XRD—XRD measurements were performed at the Institute of Earth and Environmental Sciences, University of Freiburg using a D8 Advance Powder X-ray diffractometer by Bruker Co. AXS, Karlsruhe, Germany, with a Cu-target and Cu-K_α X-rays. About 100 mg of each ash sample were ground in an agate mortar and put into a plastic sample mold. A high-precision setting (2Θ range 2–75°, step size 0.005°, and 5 s/step) was chosen to acquire patterns of sufficient quality for subsequent Rietveld investigations. Peak positions of the collected diffraction patterns were matched against the ICDD's PDF 4 Database with the DIFFRAC.EVA V5.0 software by Bruker AXS GmbH. For each identified phase, a structure file was obtained from the American Mineralogist Crystal Structure Database [4]. Structure files were then imported into the pattern resolution software TOPAS V4.2 (Bruker AXS GmbH) and Rietveld refinement was applied to determine the semi-quantitative concentrations of the crystalline phases present [32]. The amorphous content was determined by the spiking method, where 20 percent by weight (wt %) of crystalline Al_2O_3 was added to the samples. Error estimation was carried out from spiking measurements of three sample mixtures with the internal-standard method, whereby three different mixtures were prepared with various supplement amounts of potassium sulfate (K_2SO_4) and the results were then matched against a calibration curve. K_2SO_4 was chosen as it is present in all ash samples.

2.2.2. XRF analysis—The XRF device, also located at the Institute of Earth and Environmental Sciences, University of Freiburg, was a sequence PHILIPS PW2404 X-ray spectrometer equipped with a ceramic X-ray tube with a 4 kW Rh anode and six analyzer crystals for elements C to U. A standard-less method for carbonaceous rocks was chosen for

Author Manuscript Author Manuscript Author Manuscript Author Manuscript

quantification. Ash samples were prepared as fusion discs from 1 g sample material and 4 g Spectromelt A12 (66% di-lithium tetra borate, 34% lithium meta borate). Loss on ignition (LOI) was determined from weight loss during preparation of fusion discs (samples were weighed before and after fusion). Fusion was done manually over a flame with a typical temperature of about 1050 °C.

2.2.3. ICP-MS and ICP-AES—Trace element concentrations of the biomass ash samples were determined by ICP-MS and ICP-AES at an external analytical laboratory (SGS Canada Inc.). Concentrations of the following elements were determined with ICP-MS: As, Cd, Co, Cu, Hg, Ni, Pb, Sb, and Sn. Concentrations of Cr and Zn were determined by ICP-AES. Prior to the ICP analysis, ash samples were digested in aqua regia under pressure microwave treatment. Concentrations of Cr(VI) were obtained separately from ICP-AES after water leach and iron precipitation. The reporting limit for Cr(VI) concentrations from this method was 0.005 wt %.

2.2.4. Total organic carbon (TOC) with LECO carbon analyzer—The TOC content was estimated by using a LECO analyzer on dried and combusted leachates from sulfuric acid digestion. The reporting limit was 0.05 wt%.

2.2.5. SEM-EDX—Physicochemical characterization by SEM-EDX was applied for the investigation of morphological and chemical parameters of the ash particles. All SEM-EDX analyses were carried out using a LEO 1525 field emission scanning electron microscope by LEO Electron Microscopy Inc., equipped with an 80 mm^2 X-MaxN Silicon Drift Detector by Oxford Instruments and located at the Institute of Earth and Environmental Sciences, University of Freiburg. About 100 mg of each ash sample were carefully placed on an adhesive carbon pad mounted on an aluminum stub. The sample was then coated with a carbon layer of approximately 10 nm thickness under vacuum. Acceleration voltage was 15 kV and photomicrographs were captured from the secondary electron (SE) signal. EDX spectra were recorded for each distinguishable particle type in each sample. Qualitative evaluation of the EDX spectra was performed subsequent to ZAF correction (ZAF, Z = atomic number, A = absorption, F = fluorescence).

2.2.6. Ash content determination and TGA—The ash content of the DIN + wood pellets was determined from weight loss after 800 °C in a box-type furnace at the Laboratoire de Gestion des Risques et Environnement (LGRE), University of Mulhouse.

DIN + wood-pellet ash was thermally treated at temperatures up to 550, 815 and 1000 °C. After each run, the remaining ash was weighed and investigated by XRD and TGA/proximate analysis to ascertain thermally indicated reactions of organic components and decomposition and transition processes of mineral species in the ash, as well as dehydration and vaporization. TGA was conducted at a heating ramp of 5°C min^{-1} under inert air while recording weight loss every integer Kelvin.

Author Manuscript Author Manuscript Author Manuscript Author Manuscript

3. Results

3.1. Macroscopic properties

Bottom ash and corresponding FA from biomass combustion exhibited different colors and morphologic features across the various fuel and ash types (Fig. 1). Wood-chip BAs collected from St. Peter and Freiburg were macroscopically quite similar, fine-grained and homogeneous, whereas that from Ammertzwiller was heterogeneous and included unburned residues of wood. The same observations could be made for the corresponding FAs, but the Ammertzwiller cyclone ash (CA) was almost homogeneous, except for some occasional unburned wood remnants. Wood-chip BAs collected from Colmar and Rixheim included debris with diameters of several centimeters, whereby the sample from Rixheim lacked fine-grained material. The corresponding FAs from Colmar and Rixheim appeared similar and were homogeneous and fine-grained. Miscanthus bottom ash (MBA), from combustion of Miscanthus with $Ca(OH)_2$ amendment, was fine-grained and homogeneous, but the associated MCA exhibited the same structures as CA from wood chips (unburned remnants of biomass), but with a darker color.

3.2. Mineralogical compositions

Phase identification via XRD and subsequent Rietveld refinement yielded the semi-quantitative mineralogical compositions of BA and FA pairs from a selection of combustion facilities (Table 2).

Based on an assessment of the compositions listed in Table 2, quartz contents are relatively low in all BAs (≤ 6 wt%) and nearly absent in FAs, except for Ammertzwiller CA, where quartz is enriched in the FA by one order of magnitude (21 wt%) compared to the associated BA. Lime content is variable, ranging from 1 wt% (Ammertzwiller CA/ MCA and Colmar ESPA) to 13wt% (St. Peter BA and Ammertzwiller BA). Calcite and portlandite contents are also variable and range from 1 wt% (Freiburg BA) to 15 wt% (Ammertzwiller MCA) and from 1 wt% to 7 wt %, respectively. The content of C_2S, which includes the two clinker phases identified by XRD as the calcium silicates ‘alite’ (Ca_3SiO_5) and larnite (‘belite’, Ca_2SiO_4), ranges from 2 wt% (Ammertzwiller MCA) to 40 wt% (Ammertzwiller BA). The content of arcanite (sulfur-bonded potassium salt, K_2SO_4) is highly variable (1 wt% in Freiburg BA to 42 wt % in Colmar ESPA), but is always higher in FAs compared to their associated BAs. Sylvite, the chlorine-bonded potassium salt (KCl), is the only chlorine-bearing phase found via XRD and its concentrations are very low for all ash samples, except for Rixheim BAGA (3 wt%). Periclase (MgO) is relatively low (≤ 5 wt%), without notable fractionation between BA and FA. The content of amorphous material is high in all ash samples and ranges from 24 wt% (Ammertzwiller CA) to 76 wt% (Ammertzwiller MBA).

Fractionation behavior, i.e. the enrichment factor of a given phase in FA compared to the respective BA, was calculated from the XRD-Rietveld data of the three wood-chip ash pairs, and is presented in Fig. 2. Quartz is notably depleted in St. Peter ESPA and Freiburg ESPA + CA, but the arcanite concentration is enriched about ten times compared to BA. Arcanite is also enriched in Ammertzwiller CA to a similar extent. In addition, quartz and calcite are enriched, whereas lime, portlandite and C_2S are depleted in Ammertzwiller CA compared to

Author Manuscript Author Manuscript Author Manuscript Author Manuscript

the corresponding BA. Lime is also depleted in St. Peter ESPA and enriched in Freiburg ESPA + CA.

3.3. Bulk chemical composition

Similar to the large variations in mineralogical composition, the bulk chemical composition of the wood-chip ash samples varied widely (Table 3). In the following, the main constituents (expressed as oxides in wt % from XRF analyses) as well as some trace elements (expressed in ppm: As, Cd, Co, Cr, Cu, Ni, Pb, Sb Sn, Zn and Cr(VI)) from ICP-MS/ AES analyses) are described. Fractionation behavior of the major and trace elements, i.e. the enrichment factor of the elements in FAs compared to their respective BAs, was calculated from these chemical data of the three wood-chip ash pairs, and is presented in Figs. 3 and 4, respectively. MBA and MCA cannot be presented here, because preparation of XRF fusion discs failed.

SiO_2 is always more abundant in BAs, where its concentration ranges from 25.1 wt% (St. Peter BA) to 35.8 wt% (Ammertzwiller BA). Its concentration is considerably lower in FA, where most values range between 13.5 and 18.3 wt%. In ESPA from Colmar, however, a particularly low value of 2.35 wt% was observed.

The concentration of Al_2O_3 is low in all ashes, ranging from 0.56 wt % in Colmar ESPA to 5.80 wt% in Freiburg BA. Relative to its concentration in BA, Al2O3 is slightly depleted in FA from St. Peter and Freiburg, but enriched in Ammertzwiller CA.

Total Fe_2O_3 (Fe_2O_3tot) is generally low (0.79 wt% in Ammertzwiller BA to 2.53 wt% in Freiburg BA), except for Ammertzwiller CA, where it reaches 8.98 wt%, which is more than one order of magnitude higher than in the corresponding BA.

MgO ranges from 1.27 wt% to 5.84 wt% and shows no significant enrichment or depletion behavior throughout the three ash pairs.

CaO is the most abundant component in all ash samples, except for Colmar ESPA, where K_2O is dominant. The lowest concentrations can be observed in Colmar ESPA (15.7 wt%) and Rixheim BAGA (22.4 wt %), the highest in Ammertzwiller CA (55.0 wt%), with no strong fractionation between FA and BA.

K_2O is highly variable and ranges from 1.18 wt% (Ammertzwiller CA) to 32.4 wt% (Colmar ESPA). It exhibits the opposite fractionation behavior to Fe_2O_3: K_2O is enriched at about a factor of two in FA collected by ESP, and depleted by almost one order of magnitude in Ammertzwiller CA (Fig. 3).

The total of all major element components is close to 100 wt% for the BAs, whereas it is considerably lower for all FAs, with the lowest value for Colmar ESPA (58.8 wt%). LOI values range from 5.4 wt% for St. Peter BA to 30.2 wt% for Ammertzwiller CA.

Trace element concentrations of selected elements (only those were selected, were limits of Swiss regulation for wood ash in cement applications apply [36]) vary considerably across the different ash types (Table 3). Arsenic concentrations are below the detection limit of 30

Author Manuscript Author Manuscript Author Manuscript Author Manuscript

ppm, except for Rixheim BAGA and Colmar ESPA. Cadmium is below the detection limit of 0.9 ppm in all BAs, but ranges from 16 to 52 ppm in FAs. Cobalt is low in all ash samples (< 3 to 7 ppm). Chromium concentrations are slightly variable, with a notable enrichment in Ammertzwiller CA relative to the corresponding BA, in contrast to the depletion seen in FAs from St. Peter and Freiburg (Fig. 4). Copper is significantly depleted in Freiburg ESPA + CA, but notably enriched in Ammertzwiller CA. Concentrations of Ni in FAs are similar to those of Cr, but no notable fractionation is observed. Lead is low or below the detection limit of 30 ppm in BAs, but high in FAs (up to 572 ppm in Rixheim BAGA). Concentrations of Sn are low or below the detection limit of 20 ppm. Zinc concentrations are highly variable and range from 19 ppm in Ammertzwiller BA up to several thousand ppm in the FAs, with Colmar ESPA being richest in Zn (7090 ppm). There is a pronounced fractionation of Zn, with at least one order of magnitude of enrichment for St. Peter ESPA and ranging up to an enrichment factor of more than 50 for Ammertzwiller CA. Antimony and Cr(VI) concentrations are below the detection limits of 30 and 50 ppm in all ash samples, respectively. TOC values are low in all BAs and in Ammertzwiller CA, Rixheim BAGA and Colmar ESPA, but notable elevated for ESPAs from St. Peter and Freiburg (7 wt%).

3.4. Physicochemical characterization

The wood-chip ashes exhibited various complex microstructures, as observed by SEM. Selected SEM photomicrographs of four FA samples (Figs. 6–10), one from each flue gas treatment strategy, and one BA sample (St. Peter BA, Fig. 5), are presented as SE images, in which the locations of the qualitative EDX analyses are marked. In addition, standard coal FA particles are presented as a reference (Fig. 11). In the following interpretation of typical EDX spectra (Table 4), C and O were ignored, because they could not be adequately determined.

Based on SEM photomicrographs and recorded EDX spectra, woodchip BA from St. Peter consists of grains with diameters of several millimeters, as well as smaller particles with sizes down to less than one micrometer across, often forming larger domains (Fig. 5). The large grains and coarse particles angular in shape and include Ca > Si > Al as main components, as indicated by EDX (spectra 1 and 2, Fig. 5A; spectrum 4, Fig. 5B). The majority of the small particles tend to form agglomerates and typically show peaks for Ca with minor amounts of K and Mg (spectrum 3, Fig. 5A) or Ca only (spectrum 5, Fig. 5B).

Depending on the flue gas treatment strategy, the FAs exhibit considerable variation in their morphologic features, with different structures and particle shapes (Figs. 6–10).

The ESPA from St. Peter exhibits structures that are similar to those seen in the BA for the small, agglomerating particles (Fig. 6), which form domains that extend for several tens of micrometers. The EDX spectra, however, reveal different compositions: together with Ca, K seems to dominate, and additional S, Cl and small amounts of Mg, Al and Na are present. The proportions vary spatially and range from Ca > K (spectrum 1, Fig. 6A), K > Ca > S > Cl (spectrum 2, Fig. 6A), and Ca > K > P > S (spectrum 3, Fig. 6B), to K > S > Cl (spectrum 4, Fig. 6B).

Author Manuscript Author Manuscript Author Manuscript Author Manuscript

CA from Ammertzwiller is made of nearly equally sized particles with diameters not more than 20 μm (Fig. 7). Some of these particles seem to consist of agglomerates of smaller particles, but are not as fluffy as in the ESPA from St. Peter. About half of the particles have distinct spherical shapes (typical FA spheres), but with variable chemical compositions, as indicated by EDX. Compositions of the spherical particles always include Ca, Al and Si, but with varying amounts of K and/ or P (spectrum 3, Fig. 7A). Close-up views of these spheres indicate irregular coatings by fine particles (Figs. 7B; 8A), for which it was unfortunately not possible to record clean spectra due to their small size. However, some of the spheres exhibit holes (example shown in Fig. 8A), where the fine particles have accumulated. The spectrum at this location indicates K > Ca > Si > S, with small amounts of Al, Fe, and P (spectrum 2, Fig. 8A). In contrast, the sphere itself shows Si ≫ Ca > K > Al > Mg, with small amounts of Fe and P (spectrum 1, Fig. 8A). It is assumed, that K and most of the Ca in the spectrum of the sphere are due to contamination by the small particles. Based on this assumption, the EDX composition of the sphere itself would be Si > Al > Mg > Fe. Some spheres, however, also include large amounts of Fe and Ti, which are even more abundant than Si and Al (spectrum 10, Fig. 7B). The spheres are hollow, i.e. cenospheres, which is visible when the particles are broken (Fig. 8B). The non-spherical particles exhibit EDX spectra with peaks for Si, Al, Ca, K, Mg, Fe, S, and P in varying proportions (for examples, see spectra 2 and 4 – 9 in Fig. 7A and Table 4). A rather exotic type of particle is shown in Fig. 8C and D. It looks like a chain of tabular particles with a dusty surface and contains Ca as major component with additional K, S, and Cl (spectrum 3, Fig. 8C; spectrum 4, Fig. 8D).

ESPA + CA from Freiburg consists of a mixture of particle types similar to those found in Ammertzwiller CA (including spherical particles) and the small-grain agglomerations observed in the St. Peter ESPA (Fig. 9). The spherical particles are not uniformly coated by the small particles as in the pure CA; instead, the small particles form agglomerates that stick to the spheres (Fig. 9B). The agglomerates have manifold EDX compositions (see Table 4). The spectra of the uncontaminated spherical particles were easier to record than in the CA from Ammertzwiller and yield relative compositions of Si > Ca > Al > Mg > K for most of the spheres (spectrum 1, Fig. 9B).

BAGA from Rixheim (Fig. 10) has morphologic features that are similar to those of ESPA from St. Peter. Nevertheless, particles appear with margins blending with the background and it is difficult to identify individual particles. As indicated at higher magnifications, small particles seem to be fused to form larger aggregates (Fig. 10B). The EDX spectra reveal compositions varying between Ca > K > S with some Mg, Al, and Cl (spectrum 3, Fig. 10A; spectrum 5, Fig. 10B) and K > (S, Cl, Ca) (spectra 1 and 4, Fig. 10A). The only structures other than the agglomerated small particles are some spheres, whose EDX composition is a mixture of Ca, Mg, K, Si, and Al with small amounts of P, S, Cl, and Na (spectrum 2, Fig. 10A; spectrum 6, Fig. 10B).

Coal FA (CFA) consists mainly of spherical particles of different sizes up to 15 μm in diameter and occasionally some angular particles (Fig. 11). The spheres consist mostly of Si and Al, with varying S for most of the particles and, in some cases, small amounts of K and Mg (spectra 1 – 7, Fig. 11A and B).

Author Manuscript Author Manuscript Author Manuscript Author Manuscript

3.5. Thermal behavior

Thermal treatment of DIN + wood-pellet ash (produced in the 40 kW multi-fuel boiler) led to temperature-dependent weight recordings (Fig. 12), which display a complex weight-loss pattern for untreated and pretreated (pre-heated) ash. The curve of the ash pretreated at 550 °C is identical to that from the untreated ash. Both ash samples lost about twelve percent of their initial mass during heating from 25 to 1000 °C. The major weight loss started around 550 °C, and the weight-loss rate was reduced at 700 °C and again at 850 °C. For the ash that was pretreated at 815 °C, weight loss started immediately and continued to 100 °C, from where it continued at a low rate until 700 °C, beyond which the rate was elevated but not constant, resulting in a total weight loss of about four percent at 1000 °C compared to the initial weight. In contrast to this, the ash pre-treated at 1000 °C shows no weight loss across the whole temperature range.

4. Discussion

4.1 Sampling

Whenever possible, fuel and BA samples were collected along with the corresponding FA sample. Not all of the BA samples were analyzed, because some contained large pieces of extraneous materials (rocks several centimeters across) and homogenization could not be accomplished. Large debris and the absence of fine material in the BA from Rixheim can be related to high air-flow rates in the combustion chamber, typical for large-scale power plants, where small particles get suspended and transported along with the flue gas. If these BAs had been crushed and ground, or sieved, the composition would not have been representative.

4.2. Ash compositions

The compositions of the investigated biomass bulk ash and ash particles are consistent with compositional data reported in the literature [6,25,35]. In the compositional system of [35], the wood-chip BAs studied here appear in the bottom half of the triangular diagram (Fig. 13), which represents C-type ashes (high in Ca) and medium to low acidity. In the same diagram, FAs are located to the lower right relative to the corresponding BAs. Depending on the flue gas treatment strategy, FAs plot in the C-type (Ammertzwiller CA), CK-type (St. Peter ESPA and Freiburg ESPA + CA, high in Ca and K), or K-type (Rixheim BAGA and Colmar ESPA, high in K) fields. This diagram demonstrates that the compositions of all wood-chip BAs are quite similar, whereas the corresponding FA compositions vary depending on flue gas treatment strategy and boiler size. The latter is documented by the comparison of St. Peter ESPA (medium scale) and Colmar ESPA (large scale), where the compositions move from CK-type to K-type ash.

LOI values represent the weight loss during the heating prior to XRF analysis. All FAs investigated had considerably greater LOI values than their corresponding BAs, which is due to weight loss as a function of water content (through hygroscopic behavior [18]) and volatile compounds [6].

Author Manuscript Author Manuscript Author Manuscript Author Manuscript

Enrichment of Fe_2O_3tot and Cr in Ammertzwiller CA is remarkable and can be related to the presence of cenospheres in the FAs, as SEM-EDX investigations show. Zinc enrichment in all FAs is due to the high volatilization potential of Zn [17].

4.2.1. Interpretation of SEM-EDX data—Manual SEM-EDX investigations of particles cannot provide quantitative chemical results and statistically significant data due to insufficient number of investigated particles. Rather, they give a quick overview of morphological features (SE images) and qualitative chemical compositions (EDX spectra) of individual ash particles. It has to be considered, that C is a major component of the substrate material of the SEM samples (adhesive carbon pad) and was used for the coating of the samples, therefore increasing peak intensities of C.

Particles in the St. Peter BA sample (Fig. 5) can be interpreted unequivocally as extraneous minerals (carbonates, silicates), as indicated by their size and angular shape. Nevertheless, the proportions of the peak intensities in the EDX spectra are not consistent with those recorded for common silicates or carbonates. Thus, the thermal treatment during the combustion process may have initiated metamorphic processes, where carbonates underwent (partial) thermal decomposition (calcination) and incorporation of Si and Al. This interpretation is supported by the similarity of the spectra with those of clinker phases, such as di- and tricalcium silicates ($2CaO * SiO_2$ and $3CaO * SiO_2$). The smaller particles found in the BA are probably mainly calcined calcite, i.e. free lime (CaO), which was detected by XRD in this and all other ash samples. Decomposition of calcite can be observed in most SEM photomicrographs, but are best demonstrated in Figs. 5B, 8C and D. The fuzzy structures might indicate incomplete decomposition of calcite forming lime and CO_2 [22,27,30]. The micrographs in Fig. 6 show small, agglomerated particles of St. Peter ESPA, which are primarily made of Ca, K, S and Cl, pointing to free lime and salt (mainly K_2SO_4 and KCl) particles, which have probably formed as secondary condensates from the gaseous phase [25]. The spherical particles most abundant in Ammertzwiller CA (Figs. 7 and 8A and B) and sporadically found in the other FAs (Figs. 9 and 10) have the typical shapes and diameters of so-called FA particles, which can be hollow (“cenospheres”), commonly known from coal FA, where they are formed from molten mineral matter (e.g. [16,31,38]). These types of particles were also found in the coal FA sample investigated in this study (Fig. 11). Their manifold compositions, resulting from various substances adhering to their surface, make it difficult to characterize them chemically. In XRD patterns, the amorphous structure of FA spheres produces a hump-shaped background signal. Especially in biomass FAs, it is almost impossible to record their true compositions, because of the small particles attached on the surface (e.g. Fig. 7B). The presence of such spheres is important, as biomass ashes rich in cenospheres are known to have positive effects on compressive strength of the hardened mortar when added to cements [34].

4.3. Thermal behavior of mmeralogical species in wood ash

TGA data show matching weight-loss graphs for untreated DIN + wood-pellet ash and for ash after treatment at 550 °C (Fig. 12). The most likely reason for this behavior is that the initial ashing process was very close to 550 °C and no significant changes occurred during the thermal pre-treatment. The weight loss below 550 °C can be assigned to water

Author Manuscript Author Manuscript Author Manuscript Author Manuscript

vaporization (drying), which was trapped from ambient air due to the hygroscopic behavior of the ash [18]. Devolatilization is presumed to be completed after the initial ashing and is not expected to contribute to the weight loss of any thermal pre-treatment. From 550 to 700 °C, the dramatic weight loss can be assigned to the decomposition of calcite ($CaCO_3$) according to the reaction $CaCO_3(s) \rightarrow CaO\ (s) + CO_2(g)$, as described in detail by [3,11]. This assumption is confirmed by XRD analysis, which documents that calcite is present only in untreated DIN+ ash and in ash after treatment at 550 °C (Fig. 14A). Because portlandite ($Ca(OH)_2$) is present in ashes treated at 815 and 1000 °C (Fig. 14B), it can be concluded that portlandite was formed as a direct product of a reaction between free lime (CaO) and water, which was trapped from the ambient air to which the ash samples were exposed between the TGA experiments. Lime, the solid product of calcite decomposition, is most abundant in ash treated at 815 °C (Fig. 14C). The shift of this peak to higher 2 Θ in the XRD diagram may refer to the volume change due to raised temperatures of the crystal unit cell [7]. This assumption, however, cannot be fully validated due to uncertainties in the contribution of instrument shift. Weight loss observed between 815 and 1000 °C for untreated ash and ash pre-treated at 550 and 815 °C probably indicates char oxidation [24]. Nevertheless, decomposition of lignin remnants in the ash may also contribute to the weight loss in the range from 180 °C to 900 °C [8]. The formation of the calcium silicate “belite” from lime and SiO_2 may take place somewhere within the studied temperature range. Since belite consists of various minerals with many XRD reflections, there is a high chance of blurring of peak intensities due to overlapping, and the phases become difficult to distinguish (Fig. 14D). The main constituent of belite, the phase larnite (Ca2SiO4), is present in all ash samples, but is most abundant in the ash treated at 1000 °C. Therefore, it may have formed at temperatures below 550 °C, but it definitely formed at temperatures greater than 815 °C. Although it is difficult to take such small differences in intensity to make any statements (the impact of absorption is quite significant), semi-quantitative Rietveld refinement, which considers many influencing factors in addition to than absorption, supports these interpretations.

Weight loss of the ash treated at 815 °C is more linear. Nevertheless, at the beginning of heating between 25 and 100 °C, this ash lost more of its initial weight than untreated ash and ash pre-treated at 550 °C. This is believed to result from vaporization of water, which was gained from ambient air to which the ash was exposed between the experiments. The slight weight loss between 100 and 550 °C can be assigned to dehydration. The more intense dehydration for the 815 °C pre-treated sample (2% against 1%) is likely due to a stronger water sorption between experiments Beyond 550 °C, the weight-loss curve lacks the rapid fall caused by calcite decomposition, because no calcite was present anymore. The pattern between 700 and 1000 °C is similar to that of untreated ash and ash pre-treated at 550 °C, and may represent char oxidation [21].

Ash pre-treated at 1000 °C did not lose any of its weight in recognizable amounts throughout the entire temperature range. This indicates, that the ash was fully hardened and fused at 1000 °C and seems to have completely lost its hygroscopic property.

Author Manuscript Author Manuscript Author Manuscript Author Manuscript

4.4. Analytical remarks

Bulk chemical composition was obtained indirectly through the XRD-Rietveld method and was determined directly by XRF. Both methods yield useable results and only one of the two is required to analyze ash from biomass combustion. Nevertheless, it is helpful to compare the two data sets and evaluate them for consistency (Fig. S2). The oxide concentrations calculated from the mineralogical composition of the ashes, determined by XRD-Rietveld, are notably lower than those from XRF analyses (except for sulfur, which was not determined by XRF and for most species in Ammertzwiller CA). Because the oxide proportions are quite similar, there are two possible interpretations: (1) the amorphous part was overestimated with the Rietveld-refinement procedure, and (2) the ashes contain a significant fraction of very small particles and/or glass, which both appear as amorphous material in XRD patterns. It seems very unlikely that interpretation (2) is the only explanation of the discrepancies between XRD and XRF data, because of the observed proportionality of the components. However, interpretation (1) cannot account for a major part, because of the quite accurate results of the Rietveld-spiking method. This assumption is in line with the literature, where XRD-Rietveld data of FAs returned similarly high amorphous contents for both wood FA [15] and coal FA [1,9,39]. An important constituent in the amorphous part could be metakaolin, which is XRD-amorphous and forms from the decomposition of extraneous kaolinite at ~500 °C. Together with lime, calcined clay is a major reactive phase in Portland-based cements. This can explain the reduced contents of total SiO_2 derived from XRD and the absence of Al-bearing phases. Some of the Ca may be incorporated into microcrystalline lime (not identifiable in the XRD patterns), as indicated by SEM-EDX. Potassium is notably higher in XRF than in XRD-derived data, especially for BAs of St. Peter and Freiburg. Most of the above observations, however, are not valid for the Ammertzwiller CA: it is the only ash sample where values of Si and K are lower in the results from XRF compared those from XRD. Also, the amorphous content is lower than for the other ash samples. These results point to a different speciation and morphology of the ash particles, which is most likely due to the different flue gas treatment. In contrast to the other ash samples, the SiO_2 content of the Ammertzwiller CA was not under-estimated by XRD-Rietveld, but instead slightly over-estimated, probably because the crystallite sizes were large enough to produce an XRD signal. This is certainly caused by the cut-off diameter of the cyclone, which does not allow for particles < 1 μm in aerodynamic diameter to be trapped. Nevertheless, SiO_2 should be under-estimated for this sample as well, as shown with SEM-EDX images, where the amorphous glass spheres contain Si; therefore, it cannot be excluded that quartz was underestimated by the Rietveld method for this sample.

5. Conclusions

Knowledge of the mineralogical products from thermal conversion during wood combustion is very important when the ashes are considered as CRM, because some of the phases have a favorable reaction potential in cement as hydraulic to pozzolanic components. XRD, combined with Rietveld refinement, is a straight-forward method to determine the mineralogical composition, and with this result, to calculate the bulk chemical composition of wood ashes of interest for cement purposes. Nevertheless, XRD-derived bulk compositions were not in good agreement with those determined directly via XRF. It is

Author Manuscript Author Manuscript Author Manuscript Author Manuscript

assumed that both methods have considerable lack in accuracy when applied for complex materials like biomass ashes and were not suited for exact quantification. While sufficient for the purpose of this study, both methods must be adjusted to give more accurate results for industrial processes. Some of the ashes contained contaminating elements in considerable amounts, but only a few exceeded limit values as given by Swiss national regulation [36] on wood ashes that are permitted for application in cement products.

Fuel type, boiler size and flue gas treatment strategy showed major influences on ash compositions. In the case of Miscanthus straw, calcium hydroxide fuel amendments also affected the composition of the corresponding ash samples.

Supplementary Material

Refer to Web version on PubMed Central for supplementary material.

Acknowledegements

This work would not have been possible without financial support from the European Union (EU) Interreg IV 746 Program (Oberrhein, project C35 BIOCOMBUST; www.biocombust.eu). The authors would like to thank the laboratory staff at the Institute of Earth and Environmental Sciences at the University of Freiburg, Germany, especially Isolde Schmidt and Sigrid Hirth-Walther for help in chemical analysis and XRD and XRF experiments. Furthermore, we would like to thank Prof. Danilewsky from the Institute of Crystallography & Material Sciences at the University of Freiburg, Germany for help in SEM measurements. This work was supported in part by P30-ES13508 awarded by the National Institute of Environmental Health Sciences (NIEHS), United States. The findings are not the official opinions of NIEHS or NIH.

References

[1]. Chancey RT, Stutzman P, Juenger MCG, Fowler DW. Comprehensive phase characterization of crystalline and amorphous phases of a Class F fly ash. Cem Concr Res 2010;40:146–56. 10.1016/j.cemconres.2009.08.029.

[2]. Chowdhury S, Mishra M, Suganya O. The incorporation of wood waste ash as a partial cement replacement material for making structural grade concrete: an overview. Ain Shams Eng J 2015;6:429–37. 10.1016/j.asej.2014.11.005.

[3]. Criado J, Ortega A. Kinetic study of thermal decomposition of dolomite by controlled transformation rate thermal analysis (CRTA) and TG. J Therm Anal Calorim 1991;37:2369–75. 10.1007/BF01913737.

[4]. Downs RT, Hall-Wallace M. The American Mineralogist crystal structure database. Am Mineral 2003;88:247–50.

[5]. Dreissigacker HL, Surendorf F, Weber E. Technische Anleitung zur Reinhaltung der Luft: TA Luft. s.n., Koeln [etc.] 1974.

[6]. Etiégni L, Campbell AG. Physical and chemical characteristics of wood ash. Bioresour Technol 1991;37:173–8. 10.1016/0960-8524(91)90207-Z.

[7]. Fiquet G, Richet P, Montagnac G. High-temperature thermal expansion of lime, periclase, corundum and spinel. Phys Chem Miner 1999;27(2):103–11. 10.1007/s002690050246.

[8]. Gasparovic L, Koreňovâ Z, Jelemensky E. Kinetic study of wood chips decomposition by TGA. Chem Pap 2010;64:174–81. 10.2478/s11696-009-0109-4.

[9]. Ibânez J, Font O, Moreno N, Elvira JJ, Alvarez S, Querol X. Quantitative Rietveld analysis of the crystalline and amorphous phases in coal fly ashes. Fuel 2013;105:314–7. 10.1016/j.fuel.2012.06.090.

[10]. Khan AA, de Jong W, Jansens PJ, Spliethoff H. Biomass combustion in fluidized bed boilers: potential problems and remedies. Fuel Process Technol 2009;90:21–50. 10.1016/j.fuproc.2008.07.012.

Author Manuscript Author Manuscript Author Manuscript Author Manuscript

[11]. Khinast J, Brunner C, Aichinger G, Staudinger G. Reaction during Low Temperature Dry Flue Gas Desulfurization. Presented at the 15th SO2 Control Symposium 1995.

[12]. Knapp BA, Insam H. Recycling of biomass ashes. Berlin, Heidelberg: Springer Berlin Heidelberg; 2011 p. 1–16. 10.1007/978-3-642-19354-5_1.

[13]. Koppejan J, Van Loo S. The handbook of biomass combustion and co-firing. Routledge; 2012.

[14]. Koukouzas N, Hamalainen J, Papanikolaou D, Tourunen A, Jantti T. Mineralogical and elemental composition of fly ash from pilot scale fluidised bed combustion of lignite, bituminous coal, wood chips and their blends. 6th Eur Conf. Coal Res. Its Appl 2007 p. 2186–93. 10.1016/j.fuel.2007.03.036.

[15]. Koukouzas N, Ward CR, Papanikolaou D, Li Z, Ketikidis C. Quantitative evaluation of minerals in fly ashes of biomass, coal and biomass-coal mixture derived from circulating fluidised bed combustion technology. J Hazard Mater 2009;169:100–7. 10.1016/j.jhazmat.2009.03.116. [PubMed: 19410365]

[16]. Kutchko BG, Kim AG. Fly ash characterization by SEM-EDS. Fuel 2006;85:2537–44. 10.1016/j.fuel.2006.05.016.

[17]. Lind T, Valmari T, Kauppinen EI, Sfiris G, Nilsson K, Maenhaut W. Volatilization of the heavy metals during circulating fluidized bed combustion of forest residue. Environ Sci Technol 1999;33:496–502. 10.1021/es9802596.

[18]. Martin M, Tritscher T, Jurânyi Z, Heringa MF, Sierau B, Weingartner E, et al. Hygroscopic properties of fresh and aged wood burning particles. J Aerosol Sci 2013;56:15–29. 10.1016/j.jaerosci.2012.08.006.

[19]. Maschowski C, Kruspan P, Garra P, Arif AT, Troué G, Gieré R. BIOMASS ASH IN CEMENT SYSTEMS: Influence of biomass type and processing technology on mortar quality. Submitted 2019.

[20]. Miles TR, Miles TRJ, Baxter LL, Bryers RW, Jenkins BM, Oden LL. Alkali deposits found in biomass power plants: A preliminary investigation of their extent and nature. Volume 1 (No. NREL/TP-433–8142-Vol.1, SAND-96–8225-Vol.1, 251288). DOI: 10.2172/2512881995.

[21]. Morgan PA, Robertson SD, Unsworth JF. Combustion studies by thermogravimetric analysis. Fuel 1987;66:210–5. 10.1016/0016-2361(87)90243-2.

[22]. Mulokozi AM, Lugwisha E. New aspects of the decomposition kinetics of calcite. Thermochim Acta 1992;194:375–83. 10.1016/0040-6031(92)80034-T.

[23]. Combustion Nussbaumer T. and co-combustion of biomass: fundamentals, technologies, and primary measures for emission reduction. Energy Fuels 2003;17:1510–21. 10.1021/ef030031q.

[24]. Ohlemiller TJ, Kashiwagi T, Werner K. Wood gasification at fire level heat fluxes. Combust Flame 1987;69:155–70. 10.1016/0010-2180(87)90028-9.

[25]. Olanders B, Steenari B-M. Characterization of ashes from wood and straw. Biomass Bioenergy 1995;8:105–15. 10.1016/0961-9534(95)00004-Q.

[26]. Rajamma R, Ball RJ, Tarelho LAC, Allen GC, Labrincha JA, Ferreira VM. Characterisation and use of biomass fly ash in cement-based materials. J Hazard Mater 2009;172:1049–60. 10.1016/j.jhazmat.2009.07.109. [PubMed: 19699034]

[27]. Carlos Rodriguez-Navarro, Encarnacion Ruiz-Agudo, Ana Luque, Rodriguez-Navarro Alejandro B, Miguel Ortega-Huertas. Thermal decomposition of calcite: Mechanisms of formation and textural evolution of CaO nanocrystals. Am Mineral 2015;94:578 10.2138/am.2009.3021.

[28]. Schweizerischer Bundesrat. Luftreinhalte-Verordnung (LRV) 1986.

[29]. SIA SSIA SIA Merkblatt 2049, Anforderung an neue Zemente 2014.

[30]. Singh A, Dash S, Kamruddin M, Ajikumar PK, Tyagi AK, Raghunathan VS, et al. Formation of nanocrystalline calcia by the decomposition of calcite. J Am Ceram Soc 2002;85:927–32. 10.1111/j.1151-2916.2002.tb00194.x.

[31]. Smoot LD. Coal combustion and gasification. Springer-Verlag New York; 2013. Place of publication not identified.

[32]. Taylor JC. Computer programs for standardless quantitative analysis of minerals using the full powder diffraction profile. Powder Diffr 1991;6:2–9. 10.1017/S0885715600016778.

Author Manuscript Author Manuscript Author Manuscript Author Manuscript

[33]. Taylor M, Tam C, Gielen D. Energy efficiency and CO2 emissions from the global cement industry. Korea 2006;50:61–7.

[34]. Tkaczewska E, Mróz R, Łój G. Coal-biomass fly ashes for cement production of CEM II/A-V 42.5R. Constr Build Mater 2012;28:633–9. https://doi.Org/10.1016/j.conbuildmat.2011.10.022.

[35]. Vassilev SV, Baxter D, Andersen LK, Vassileva CG. An overview of the chemical composition of biomass. Fuel 2010;89:913–33. https://doi.Org/10.1016/j.fuel.2009.10.022.

[36]. Verordnung vom 4. Dezember 2015 über die Vermeidung und die Entsorgung von Abfällen (Abfallverordnung, VVEA), 2016. 814.600.

[37]. Wang S, Baxter L. Comprehensive study of biomass fly ash in concrete: strength, microscopy, kinetics and durability. Fuel Process Technol 2007;88:1165–70. 10.1016/j.fuproc.2007.06.016.

[38]. Wang S, Baxter L, Fonseca F. Biomass fly ash in concrete: SEM, EDX and ESEM analysis. Fuel 2008;87:372–9. 10.1016/j.fuel.2007.05.024.

[39]. Ward CR, French D. Determination of glass content and estimation of glass composition in fly ash using quantitative X-ray diffractometry. In: Spec. Issue 2005 World Coal Ash Conf vol. 85, 2268–2277. DOI:10.1016/j.fuel.2005.12.026 2006.

Author Manuscript Author Manuscript Author Manuscript Author Manuscript

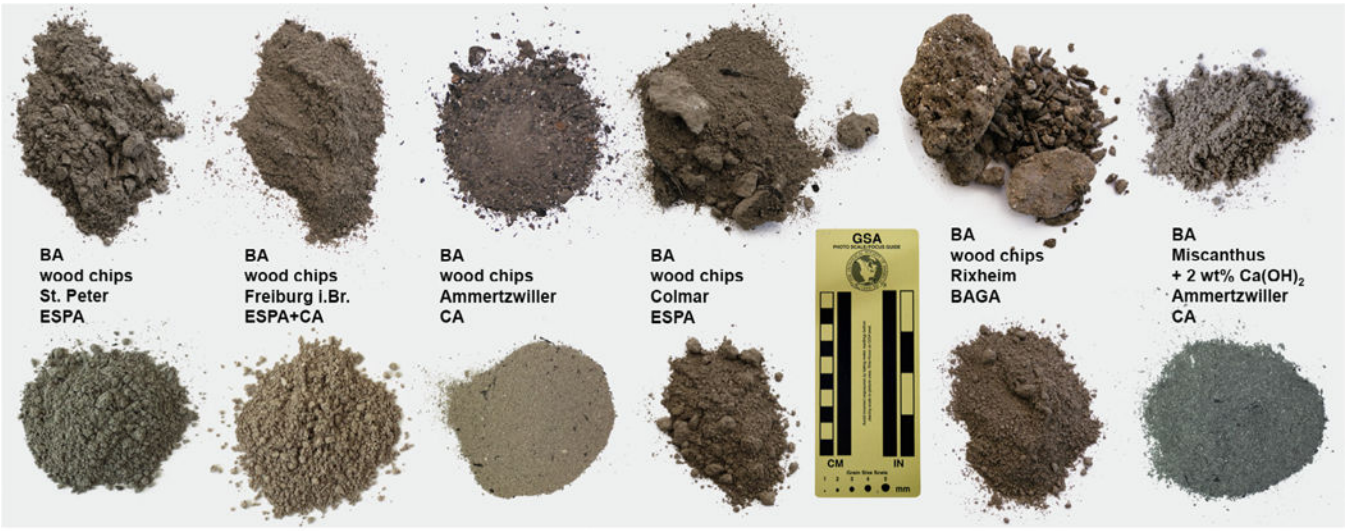

Fig. 1.

Photographs of bottom ashes (BA, top row) and corresponding fly ashes (FA, bottom row) from the five biomass power plants.

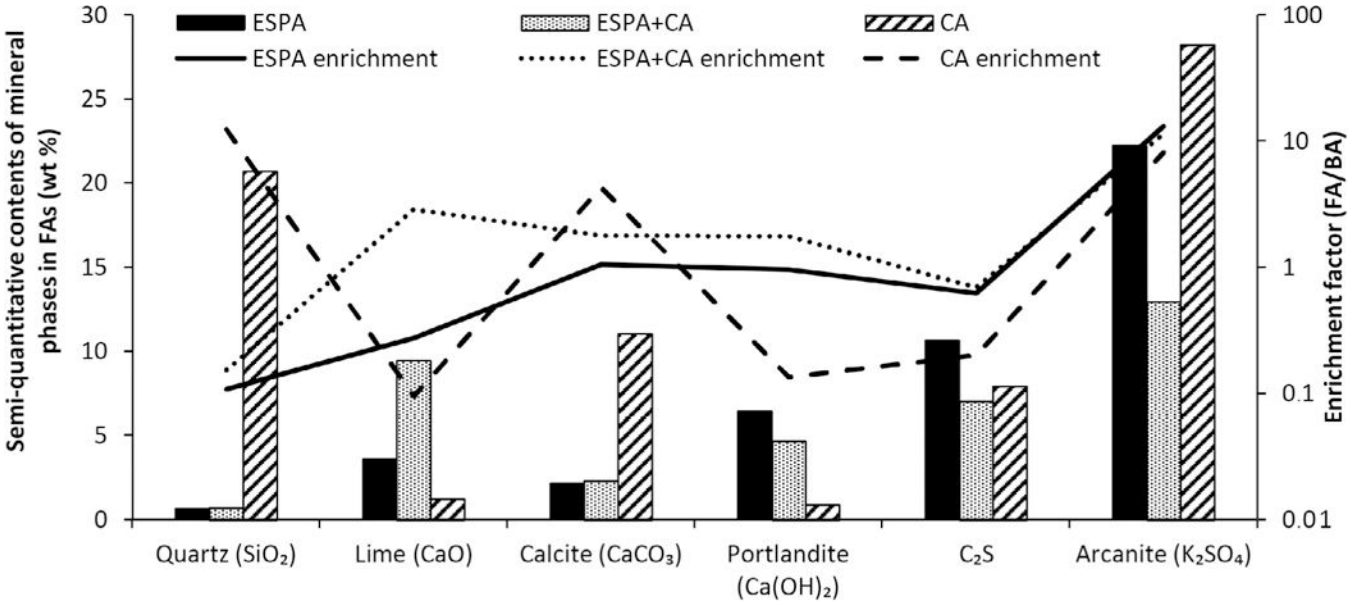

Fig. 2.

Semi-quantitative contents of mineral phases in FA from St. Peter (ESPA), Freiburg (ESPA + CA) and Ammertzwiller (CA) as identified by XRD and quantified by subsequent Rietveld refinement; Enrichment factors calculated according xFA / xBA; abundance in wt %.

Author Manuscript Author Manuscript Author Manuscript Author Manuscript

Author Manuscript Author Manuscript Author Manuscript Author Manuscript

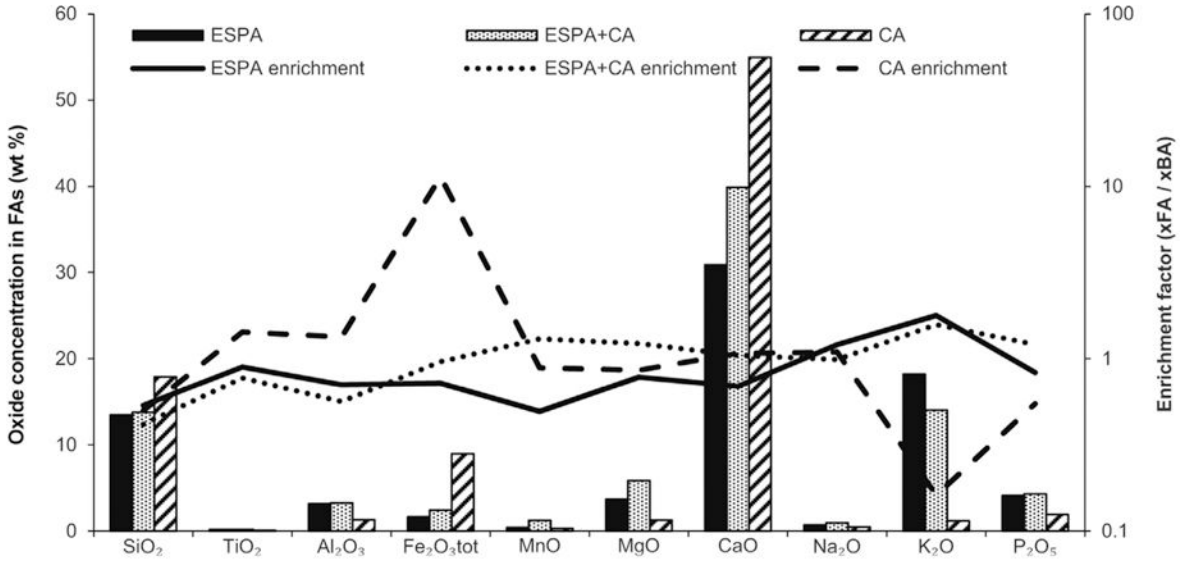

Fig. 3.

Oxide concentrations (XRF data, in wt %) in FA of St. Peter (ESPA), Freiburg (ESPA + CA) and Ammertzwiller (CA). Enrichment factors calculated according xFA/xBA.

Author Manuscript Author Manuscript Author Manuscript Author Manuscript

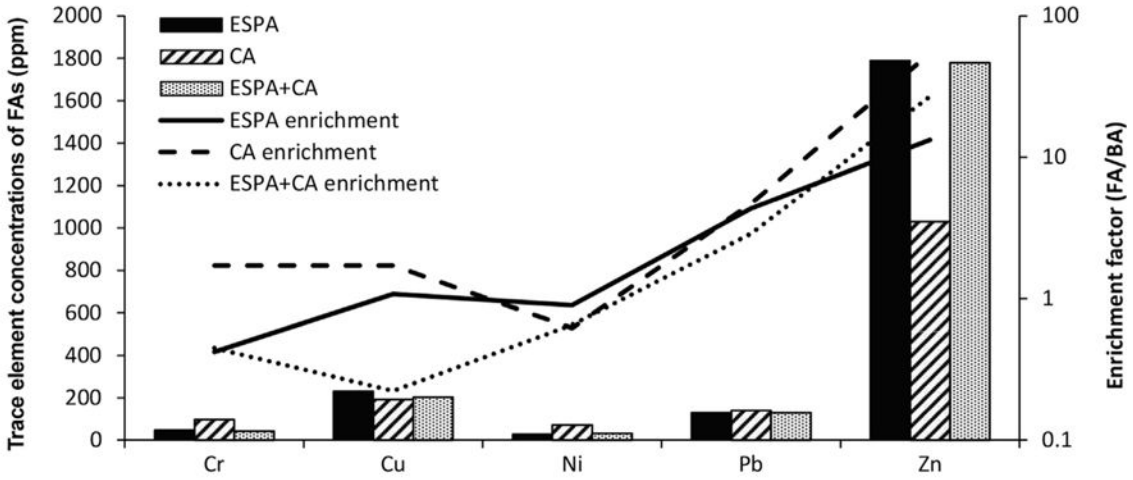

Fig. 4.

Trace element concentrations (ICP-MS/AES data, in ppm) in FA of St. Peter (ESPA), Freiburg (ESPA + CA) and Ammertzwiller (CA). Enrichment factors calculated according xFA/xBA.

Author Manuscript Author Manuscript Author Manuscript Author Manuscript

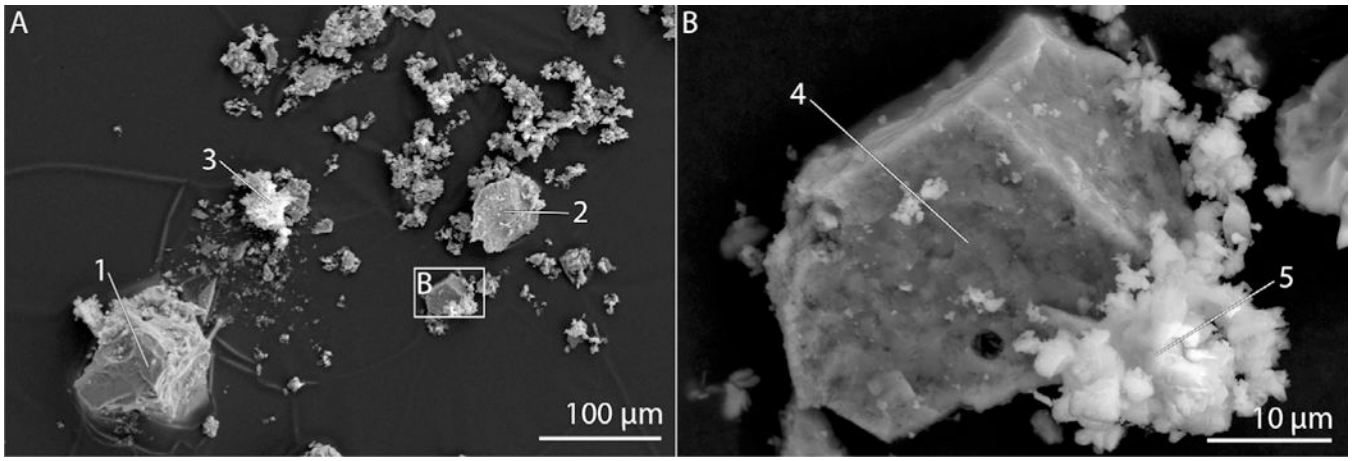

Fig. 5.

SEM SE photomicrographs of wood-chip BA particles from St. Peter; B) magnified region in A); numbers indicate locations of recorded EDX spectra.

Author Manuscript Author Manuscript Author Manuscript Author Manuscript

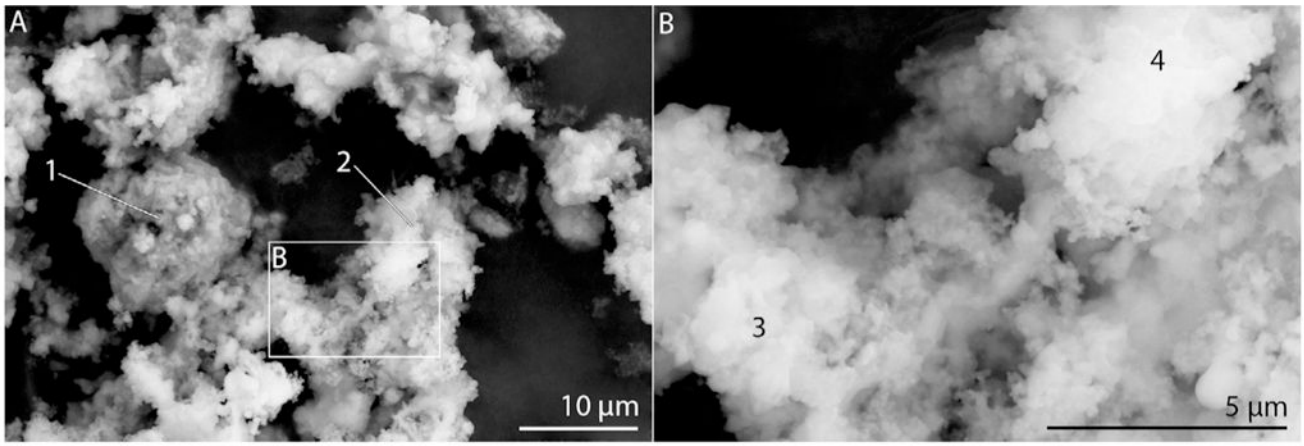

Fig. 6.

SEM SE photomicrographs of wood-chip ESP ash particles from St. Peter; B) magnified region in A); numbers indicate locations of recorded EDX spectra.

Author Manuscript Author Manuscript Author Manuscript Author Manuscript

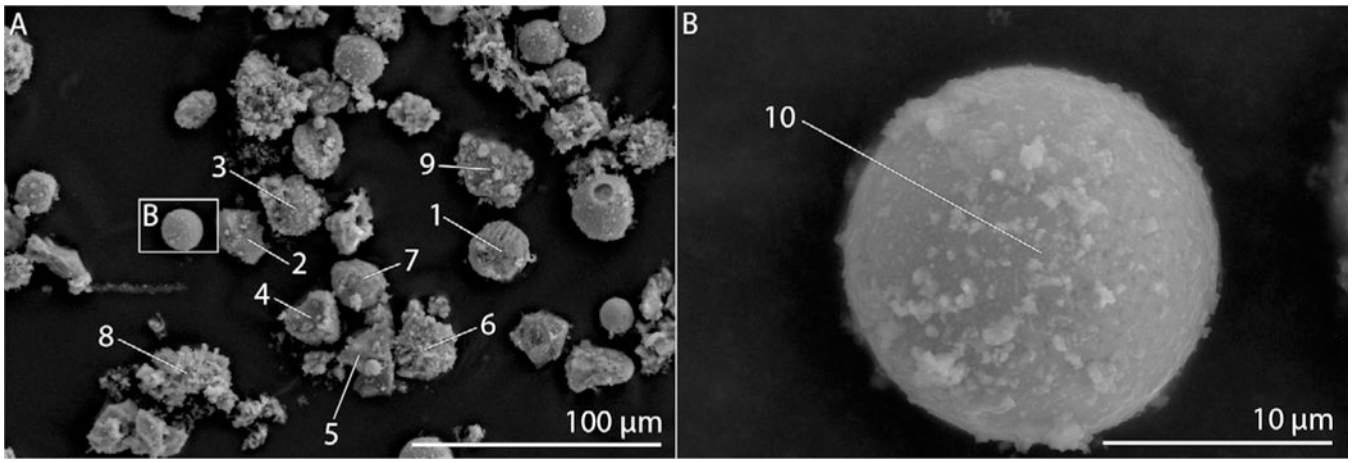

Fig. 7.

SEM SE photomicrographs of wood-chip CA particles from Ammertzwiller; B) magnified region in A); numbers indicate locations of recorded EDX spectra.

Author Manuscript Author Manuscript Author Manuscript Author Manuscript

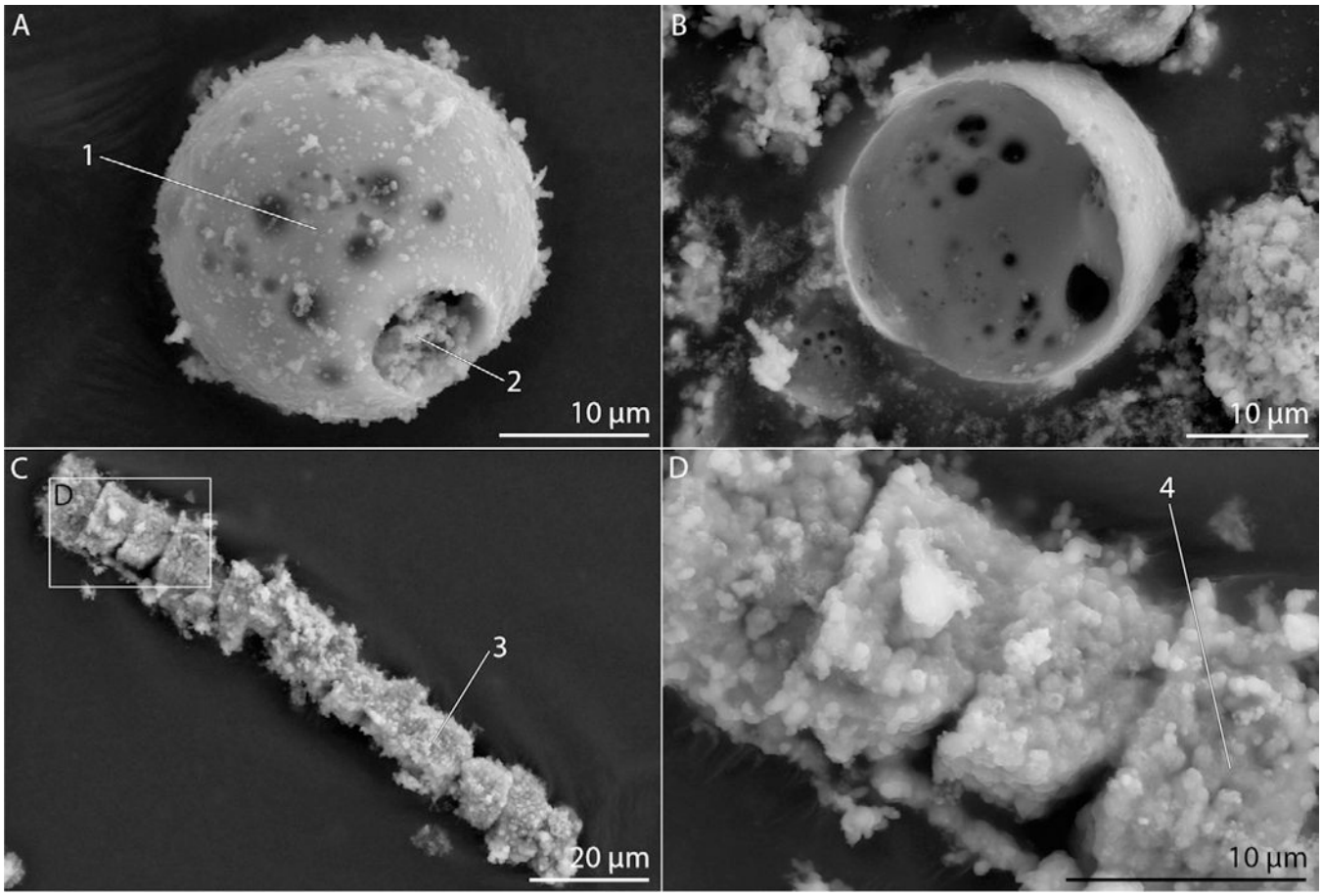

Fig. 8.

SEM SE photomicrographs of wood-chip CA particles from Ammertzwiller; A) to C) selections of individual particles; D) magnified region in C); numbers indicate locations of recorded EDX spectra.

Author Manuscript Author Manuscript Author Manuscript Author Manuscript

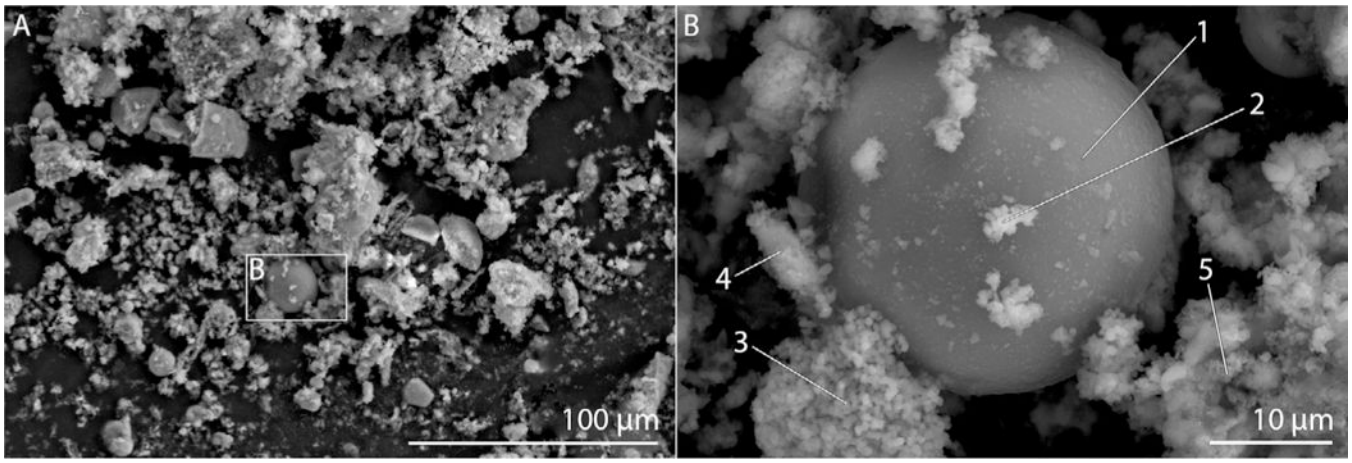

Fig. 9.
SEM SE photomicrographs of wood-chip ESPA+CA particles from Freiburg; B) magnified region in A); numbers indicate locations of recorded EDX spectra.

Author Manuscript Author Manuscript Author Manuscript Author Manuscript

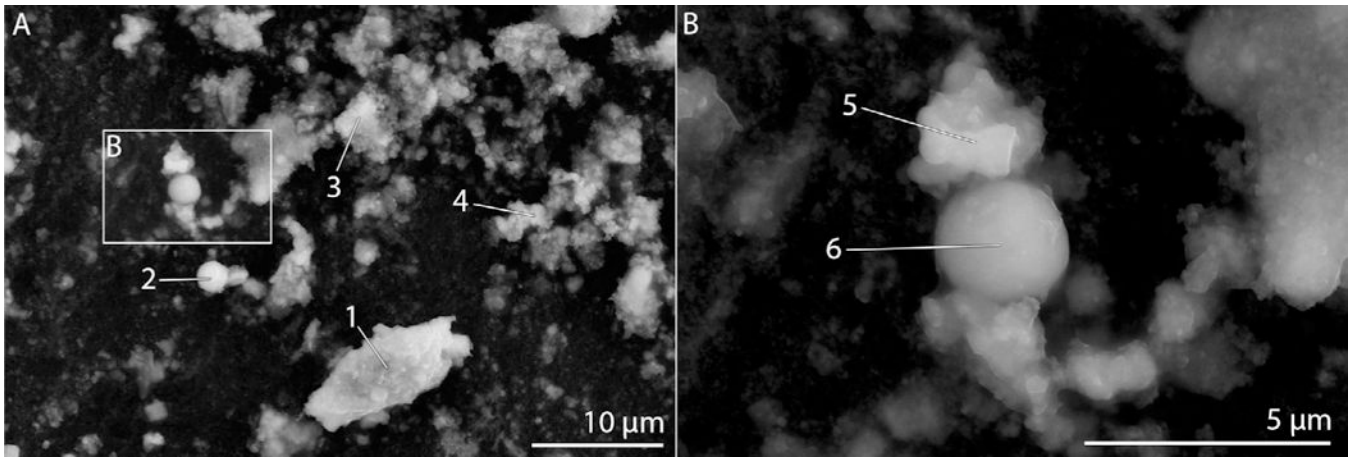

Fig. 10.

SEM SE photomicrographs of wood-chip BAGA particles from Rixheim; B) magnified region in A); numbers indicate locations of recorded EDX spectra.

Author Manuscript Author Manuscript Author Manuscript Author Manuscript

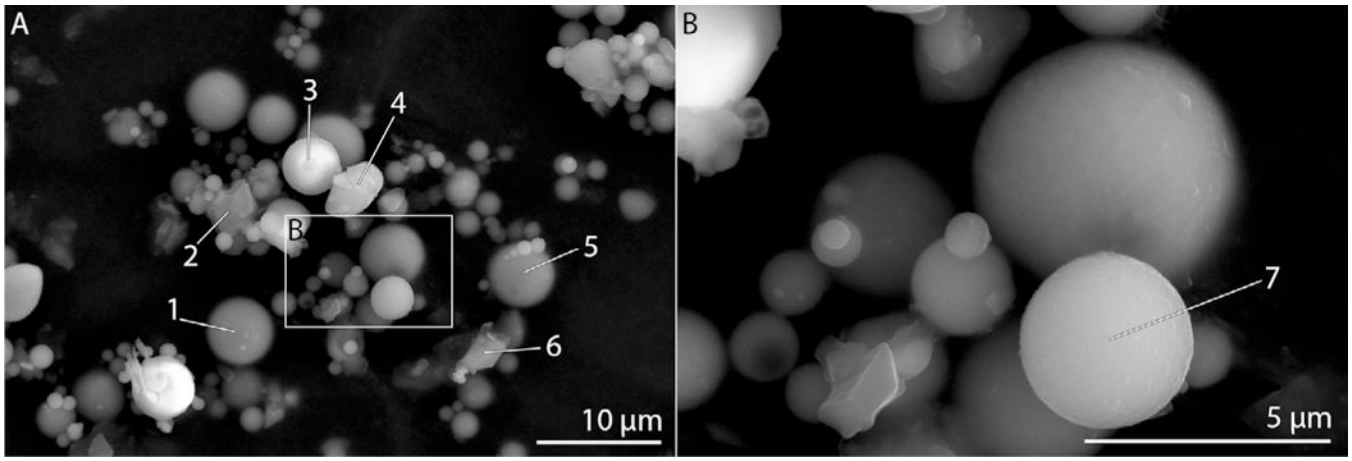

Fig. 11.
SEM SE photomicrographs of standard coal fly ash particles; B) magnified region in A); numbers indicate locations of recorded EDX spectra.

Author Manuscript Author Manuscript Author Manuscript Author Manuscript

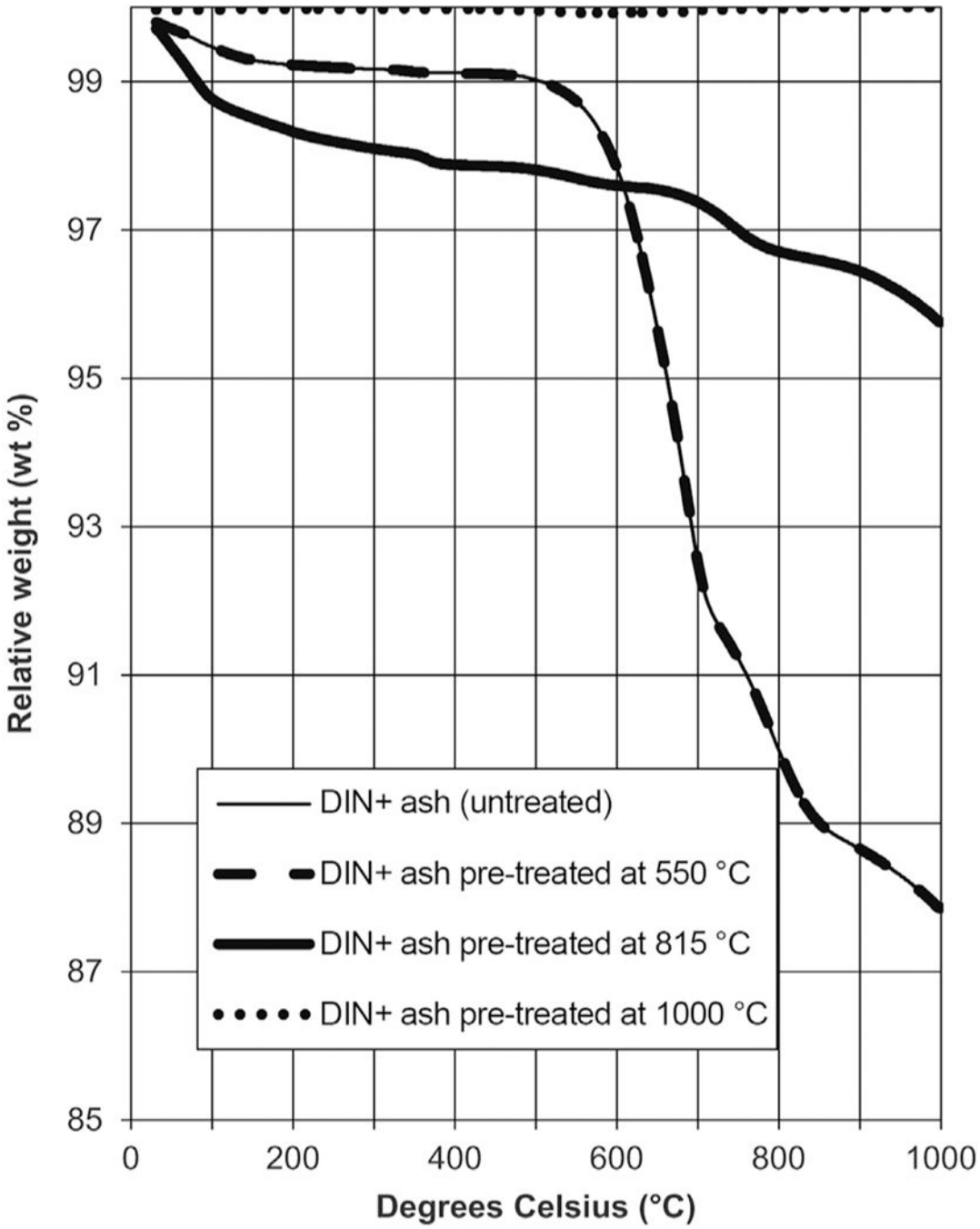

Fig. 12.

TGA cycles of untreated and pre-treated DIN + wood-pellet ash; Relative weight in wt % ($g \cdot 100 g^{-1}$).

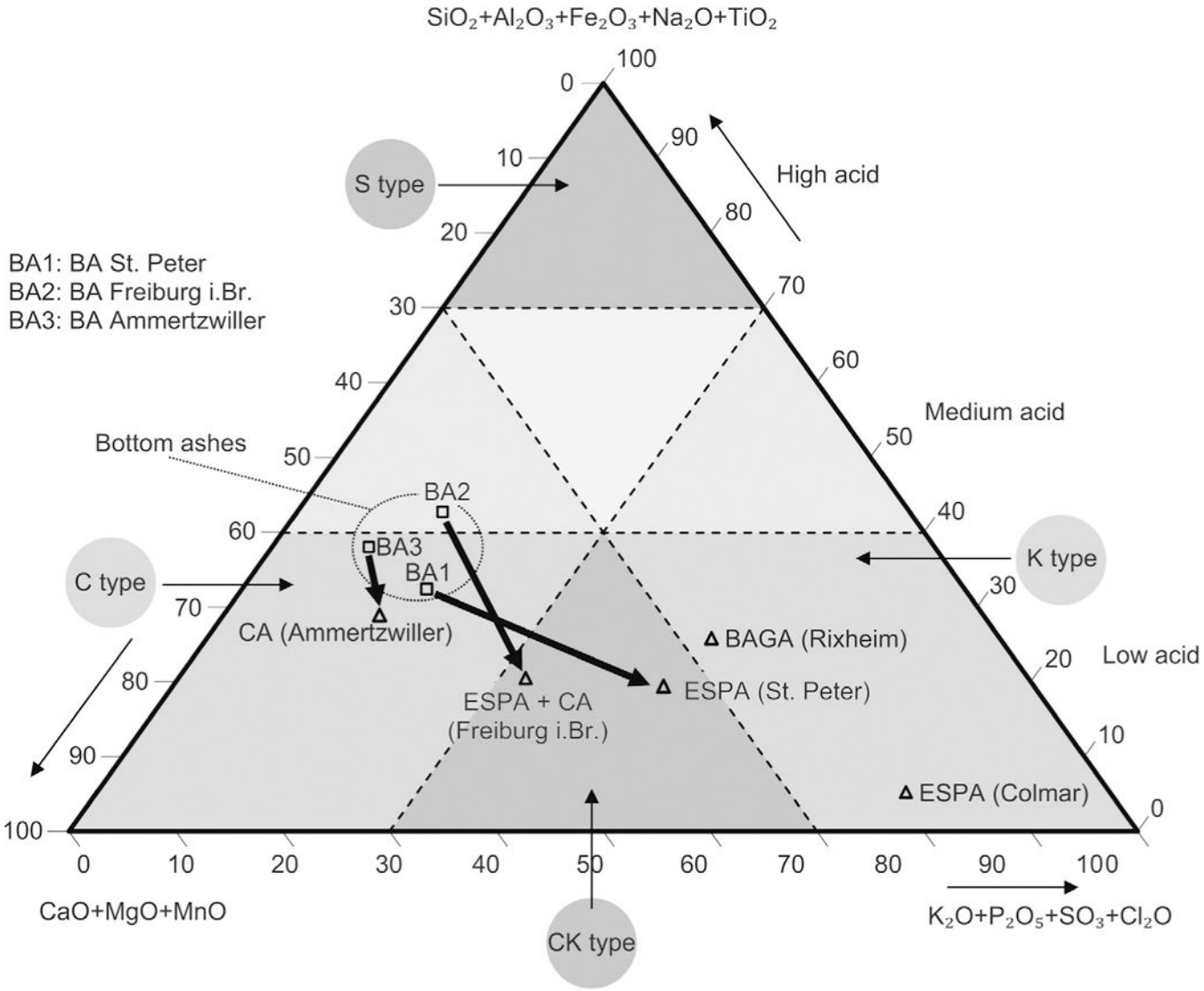

Fig. 13.

Locations of ash samples in the chemical classification system of biomass according to [33,35]; arrows indicate BA – FA pairs; values in wt %

Author Manuscript Author Manuscript Author Manuscript Author Manuscript

Author Manuscript Author Manuscript Author Manuscript Author Manuscript

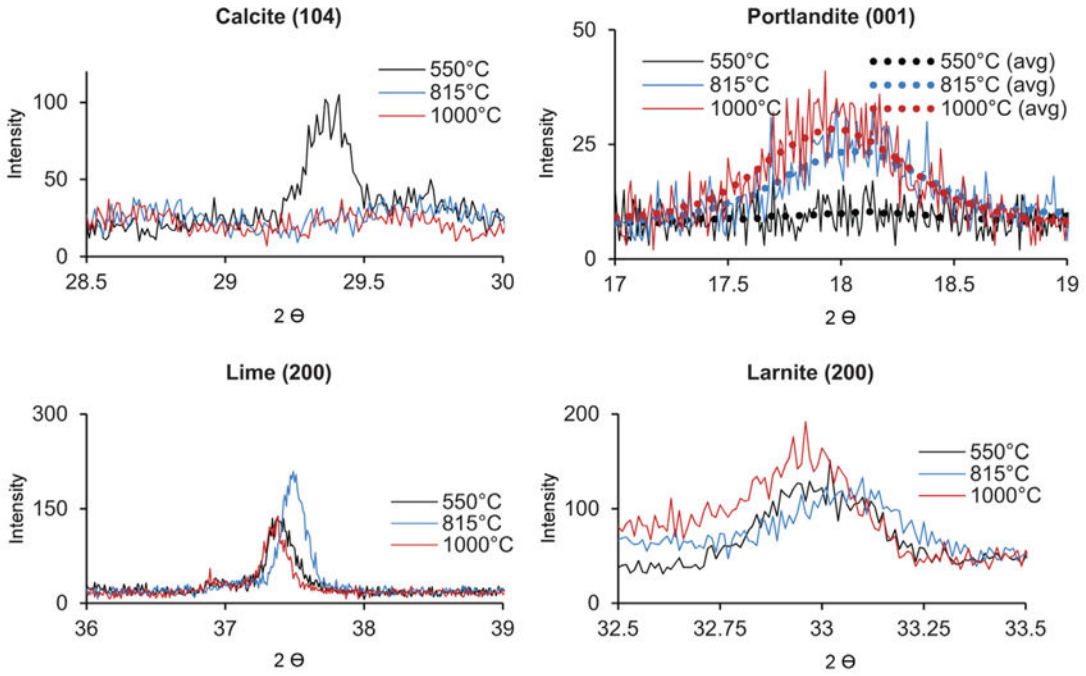

Fig. 14.

XRD intensity peaks of selected hkl locations (2Θ angle) of mineral species from TGA experiments of DIN+ wood-pellet ash; hkl-values of corresponding mineral in brackets; avg: moving average on the basis of 50 values (± 25).

Author Manuscript Author Manuscript Author Manuscript Author Manuscript

Table 1

Fly ash sample sources with corresponding installation site, fuel and boiler type, total thermal power and flue gas treatment strategy; CYC: cyclone; ESP: electrostatic precipitator; BAG: baghouse filter.

Installation site	Fuel type	Boiler type	Total thermal power	Flue gas treatment device sampled
Ammertzwiller (France)	Wood chips	Fixed bed	400 kW	CYC
Ammertzwiller (France)	Miscanthus straw + 2wt% $Ca(OH)_2$	Fixed bed	400 kW	CYC
St. Peter (Germany)	Wood chips	Fixed bed	1.7 MW	ESP
Freiburg i.Br. (Germany)	Wood chips	Fixed bed	2.3 MW	ESP + CYC
Rixheim (France)	Wood chips	Fixed bed	2.8 MW	BAG
Colmar (France)	Wood chips	Fixed bed	8.0 MW	ESP

Author Manuscript Author Manuscript Author Manuscript Author Manuscript

Table 2

Semi-quantitative mineralogical composition of ash samples obtained via XRD and subsequent Rietveld refinement. BA: bottom ash; ESPA: electrostatic precipitator ash; CA: cyclone ash; MS: Miscanthus straw; MBA: Miscanthus bottom ash; MCA: Miscanthus cyclone ash. Values in g·100 g^{-1} (wt %); n.d.: not detected.

	St. Peter (wood chips)		Freiburg (wood chips)		Ammertzwiller (wood chips)		Ammertzwiller (MS + 2wt% Ca $(OH)_2$)		Rixheim (wood chips)	Colmar (wood chips)
	BA	**ESPA**	**BA**	**ESPA + CA**	**BA**	**CA**	**MBA**	**MCA**	**BAGA**	**ESPA**
Quartz (SiO_2)	6	1	5	1	2	21	2	n.d.	1	n.d.
Lime (CaO)	13	4	3	9	13	1	6	1	4	1
Calcite ($CaCO_3$)	2	2	1	2	3	11	2	15	3	3
Portlandite ($Ca(OH)_2$)	7	6	3	5	7	1	1	7	1	1
C_2S (alite + belite)	17	11	10	7	40	8	12	2	2	2
Arcanite (K_2SO_4)	2	22	1	13	3	28	1	2	23	42
Sylvite(KCl)	n.d.	1	n.d.	1	n.d.	n.d.	n.d.	n.d.	3	1
Periclase (MgO)	3	2	2	3	5	4	n.d.	n.d.	2	2
Other	1	n.d.	1	1	n.d.	1	n.d.	1	n.d.	1
Amorphous	49	52	73	60	28	24	76	73	61	47

Author Manuscript Author Manuscript Author Manuscript Author Manuscript

Table 3

Concentrations of major and selected trace elements in the wood-chip ash samples obtained via XRF and ICP-MS/AES. BA: bottom ash; ESPA: electrostatic precipitator ash; CA: cyclone ash; BAGA: baghouse filter ash; LOI: loss on ignition; values in g·100 g^{-1} (wt %) for major element components and LOI, mg·1 kg^{-1} (ppm) for trace elements; major elements calculated as oxides; n.d.: not detected.

Major	**St. Peter (wood chips)**		**Freiburg (wood chips)**		**Ammertzwiller (wood chips)**		**Rixheim (wood chips)**	**Colmar (wood chips)**
component	**BA**	**ESPA**	**BA**	**ESPA+CA**	**BA**	**CA**	**BAGA**	**ESPA**
SiO_2	25.1	13.5	33.1	13.8	35.8	17.9	18.3	2.35
TiO_2	0.19	0.17	0.22	0.17	0.07	0.10	0.17	0.03
Al_2O_3	4.51	3.18	5.80	3.27	0.98	1.31	3.13	0.56
Fe_2O_3tot	2.28	1.64	2.53	2.43	0.79	8.98	2.31	0.85
MnO	0.83	0.41	0.95	1.24	0.35	0.31	0.88	0.73
MgO	4.73	3.70	4.76	5.84	1.48	1.27	3.76	2.89
CaO	44.6	30.9	38.1	39.9	51.1	55.0	22.4	15.7
Na_2O	0.58	0.70	0.96	0.95	0.43	0.47	1.90	1.34
KO	10.2	18.2	8.90	14.0	7.31	1.18	18.9	32.4
P_2O_5	4.96	4.13	3.56	4.31	3.51	1.92	2.43	2.04
Total	**98.1**	**76.5**	**98.9**	**85.9**	**102**	**88.4**	**74.2**	**58.8**
LOI	**5.40**	**21.1**	**9.41**	**15.0**	**3.51**	**30.2**	**12.0**	**16.2**
Trace	St. Peter		Freiburg		Ammertzwiller		Rixheim	Colmar
elements	**BA**	**ESPA**	**BA**	**ESPA+CA**	**BA**	**CA**	**BAGA**	**ESPA**
As	< 30	< 30	< 30	< 30	< 30	< 30	125	43
Cd	< 0.9	16	< 0.9	16	< 0.9	25	30	52
Co	7	5	7	5	6	7	6	< 3
Cr	114	48	96	43	57	98	69	50
Cu	214	231	912	204	88	193	259	281
Ni	31	28	49	32	116	72	33	34
Pb	< 30	131	45	130	< 30	142	572	341
Sb	< 30	< 30	< 30	< 30	< 30	< 30	< 30	< 30
Sn	< 20	< 20	59	< 20	< 20	< 20	28	< 20

Author Manuscript Author Manuscript Author Manuscript Author Manuscript

Major	St. Peter (wood chips)		Freiburg (wood chips)		Ammertzwiller (wood chips)		Rixheim (wood chips)	Colmar (wood chips)
component	**BA**	**ESPA**	**BA**	**ESPA+CA**	**BA**	**CA**	**BAGA**	**ESPA**
Zn	135	1790	66	1780	19	1030	4570	7090
Cr(VI)	< 50	< 50	< 50	< 50	< 50	< 50	< 50	< 50
TOC Leco (values in wt %)	0	7	0	7	2	2	1	0

Author Manuscript Author Manuscript Author Manuscript Author Manuscript

Table 4

Qualitative interpretations of the EDX spectra intensities, showing only major components; O and C ignored; Sp. Nr.=spectrum number as indicated on Figs. 5–11; elements in parentheses have similar intensities. BA: bottom ash; ESPA: electrostatic precipitator ash; CA: cyclone ash; BAGA: baghouse filter ash.

Sp. Nr.	St. Peter BA Fig. 5	St. Peter ESPA Fig. 6	Ammertzwiller CA Fig. 7	Ammertzwiller CA Fig. 8	Freiburg ESPA+CA Fig. 9	Rixheim BAGA Fig. 10	Coal fly ash CFA Fig. 11
1	Ca > Si > Al	Ca > K	Mg≫K > S	Si≫Ca > K > Al > Mg	Si > Ca > Al > Mg > K	K > (S, Cl, Ca)	(Si, Al)≫K
2	Ca > Si > Al	K > Ca > S > Cl	Si≫ (K, Al, S)	K > Ca > Si > S	Ca > Si > K > Al > Mg	Ca > Mg > K > Si > Al	(Si, Al)≫ (K, S, Mg)
3	Ca≫(K, Mg)	Ca > K > P > S	Ca > Si > Al > K > P	Ca > K > S > Cl	Ca≫K	Ca > K > S > Mg > Al > Cl	(Si, Al)≫(K, Mg)
4	Ca > Si > Al	K > S > Cl	Si≫(K, Al)	Ca > K > S > Cl	Ca≫K > (Mg, Si, S)	K > (S, Cl, Ca)	(Si, Al)≫K
5	Ca		Si≫ (K, Al)		Ca≫K > (Mg, P)	Ca > K > S > Mg > Al > Cl	(Si, Al)≫(K, Mg)
6			Si > K≫(Ca, S)			Ca > Mg > K > Si > Al	Si > Al > S > K
7			Si≫(K, Al)				(Si, Al)≫K
8			K> Ca > S > P > Mg				
9			K > Cl > Si > Al > S > K				
10			Fe > Ti > Si > Al				